Location of modulatory β subunits in BK potassium channels

Guoxia Liu,[1] Xiaowei Niu,[1,3] Roland S. Wu,[1] Neelesh Chudasama,[1] Yongneng Yao,[3] Xin Jin,[3] Richard Weinberg,[1] Sergey I. Zakharov,[1] Howard Motoike,[2] Steven O. Marx,[1,7] and Arthur Karlin[3,4,5,6]

[1]Division of Cardiology, Department of Medicine, and [2]Department of Natural and Applied Sciences, LaGuardia Community College, Long Island City, NY 11101

[3]Center for Molecular Recognition, [4]Department of Biochemistry and Molecular Biophysics, [5]Department of Physiology and Cellular Biophysics, [6]Department of Neurology, and [7]Department of Pharmacology, College of Physicians and Surgeons, Columbia University, New York, NY 10032

Large-conductance voltage- and calcium-activated potassium (BK) channels contain four pore-forming α subunits and four modulatory β subunits. From the extents of disulfide cross-linking in channels on the cell surface between cysteine (Cys) substituted for residues in the first turns in the membrane of the S0 transmembrane (TM) helix, unique to BK α, and of the voltage-sensing domain TM helices S1–S4, we infer that S0 is next to S3 and S4, but not to S1 and S2. Furthermore, of the two β1 TM helices, TM2 is next to S0, and TM1 is next to TM2. Coexpression of α with two substituted Cys's, one in S0 and one in S2, and β1 also with two substituted Cys's, one in TM1 and one in TM2, resulted in two αs cross-linked by one β. Thus, each β lies between and can interact with the voltage-sensing domains of two adjacent α subunits.

INTRODUCTION

Large-conductance voltage- and calcium-activated potassium (BK) channels are negative feedback regulators of cytoplasmic Ca^{2+}. BK channels are a complex of four α subunits and four β subunits (Butler et al., 1993; Knaus et al., 1994b). The α subunit contains the S1 through S6 transmembrane (TM) helices conserved in all voltage-gated K^+ channels and, in addition, a seventh TM helix, S0 (Wallner et al., 1996) (Fig. 1 A). β subunits, which tune the channel to its cell-specific roles, have cytoplasmic N-terminal and C-terminal segments, two TM helices, TM1 and TM2, and an extracellular loop of ∼120 residues (Knaus et al., 1994b; Wallner et al., 1999; Brenner et al., 2000; Uebele et al., 2000) (Fig. 1 A). Compared with the channel formed of α subunits alone, the addition of β1 enhances the Ca^{2+}-induced leftward shift in the V_{50} for channel activation and slows both activation and deactivation of the channel.

We previously assessed by disulfide cross-linking the proximities of the extracellular flank of S0 to the flanks of S1–S6 and of the flanks of S0–S6 to the flanks of TM1 and TM2 (Liu et al., 2008a,b). We found that the extracellular flank of S0 was closest to the four-residue loop between S3 and S4 and also formed cross-links with the flanks of S1 and S2 (Liu et al., 2008a). We also found with β1 (Liu et al., 2008b) and with β4 (Wu et al., 2009) that the flank of TM1 was closest to the flanks of S1 and S2, and the flank of TM2 was closest to the flank of S0. Wallner et al. (1996) had previously suggested that S0 and its preceding N-terminal residues act as a docking site for β1.

In the context of a computed model of Kv1.2 in the closed state (Yarov-Yarovoy et al., 2006), we placed the extracellular end of S0 in a crevice between S2 and S3, TM2 next to S0, and TM1, separated from TM2, outside of the S1–S4 bundle, next to S1 and S2 (Liu et al., 2008a). Our placement of S0 was dictated in part by the lack of cross-linking of the S0 flank to the flanks of S5 and S6. We recently noted that in the context of the crystal structure of the Kv1.2/Kv2.1 chimera in the open state (Long et al., 2005), our results were also consistent with S0 next to S3–S4, outside of the voltage sensor bundle (Wu et al., 2009). Based on cryoelectron microscopy and single-particle reconstruction, Wang and Sigworth (2009) found a large protrusion at the periphery of the voltage sensor domain, which they attributed to the S0 TM helix and the flanking N-terminal residues.

We have now examined cross-linking between cysteine (Cys) substituted in the first helical turns of S0–S4, TM1, and TM2 in the membrane domain. We also tested whether two αs could be cross-linked through

G. Liu and X. Niu contributed equally to this paper.

Correspondence to Arthur Karlin: ak12@columbia.edu; or Steven Marx: sm460@columbia.edu

Abbreviations used in this paper: BK, large-conductance voltage- and calcium-activated potassium; Cys, cysteine; HRP, horseradish peroxidase; HRV, human rhinovirus; PDI, protein disulfide isomerase; pWT, pseudo–wild-type; TM, transmembrane; WT, wild-type.

The Rockefeller University Press $30.00
J. Gen. Physiol. Vol. 135 No. 5 449–459
www.jgp.org/cgi/doi/10.1085/jgp.201010417

one β and whether TM1 and TM2 are contiguous. The results locate S0 outside of S1–S4 and β TM1 and TM2 between adjacent voltage sensor domains.

MATERIALS AND METHODS

Constructs

Mutants of the mouse BK α subunit (mSlo1 and KCNMA1; GenBank/EMBL/DDBJ accession no. NM_010610) were generated in three different backgrounds. Pseudo–wild-type (pWT) α has the two extracellular Cys's, Cys14 and Cys141, mutated to Ala. FLAG-pWT α has the tag and linker (MDYKDDDDKSPGDS) added to the pWT N terminus. FLAG-HRV-pWT α has the human rhinovirus (HRV)-3C protease consensus cleavage site, LEVLFQGP, inserted in the S0–S1 loop of FLAG-pWT α, with the mutation A89L and the insertion LFQGP between Val91 and Gly92 (Liu et al., 2008a) (Fig. 1 A). Cys substitutions in mouse β1 subunit (KCNMB1) were made in three different background constructs: pWT β1 contains the mutations C18A and C26A, FLAG-pWT β1 contains an N-terminal FLAG tag, and HIS-FLAG-pWT β1 has an N-terminal six-His tag preceding the FLAG tag (MGGSHHHHHHGDYKDDDDKGS-pWT β1). All β1 constructs are *N*-glycosylated at two sites, adding ∼10 kD to their apparent molecular masses.

Expression

HEK293 cells were transfected with the appropriate α and β1 constructs, surface biotinylated with 1 mM sulfosuccinimidyl-6-(biotinamido) hexanoate) (sulfoNHS-LC-biotin; Thermo Fisher Scientific) in DPBS, pH 7.4, and solubilized in 2 mM *N*-ethylmaleimide and complete protease inhibitors (Roche) in lysis buffer (1% Triton X-100, 150 mM NaCl, 50 mM Tris, and 1 mM EDTA), as described previously (Liu et al., 2008a).

Intrasubunit cross-linking of α

The extent of cross-linking between Cys substituted in S0 and S1–S4 of FLAG-HRV-pWT α was determined as described previously (Liu et al., 2008a). In brief, after the cells were surface biotinylated and lysed, the lysate was mixed with Neutravidin-Sepharose beads (Thermo Fisher Scientific) and washed extensively. The beads were mixed with HRV-3C protease (EMD) overnight at 4°C. Protein was eluted from the beads in 4 M urea, 2% SDS. Half of each sample was reduced with 10 mM DTT. The unreduced and the reduced portions were electrophoresed and transferred to nitrocellulose. α-Containing components were visualized by sequential treatment with anti–BK α C-terminal epitope antibody (BD), horseradish peroxidase (HRP)-conjugated secondary antibody, and ECL reagent (Thermo Scientific). We quantitated the chemiluminescence with a CCD camera (Carestream; Kodak) and ImageQuant software (Molecular Dynamics). For each sample, the efficiency of HRV-3C cleavage was determined from the integrated luminescence of the bands from a DTT-reduced aliquot (Fig. 1, C–F, second lanes). The fraction of cross-linked α in the unreduced aliquot was calculated as 1 minus the fraction that was not cross-linked, which in turn was the fraction in the ∼110-kD band divided by the efficiency of cleavage (Fig. 1, C–F, first lanes) (Liu et al., 2008a).

Cross-linking α and β1

We determined the extent of cross-linking between Cys-substituted FLAG-pWT α and pWT β1 subunits as described previously (Liu et al., 2008b). In brief, surface cell proteins were biotinylated, cells were lysed, and the lysate was mixed with Neutravidin-Sepharose beads. The beads were washed, the bound protein was eluted, and the samples were electrophoresed, transferred to nitrocellulose, and immunoblotted as described above. We calculated the extent of cross-linking from the integrated luminescence from the band at apparent mass, ∼160 kD, divided by the sum of the integrated luminescence of the bands at ∼130 and ∼160 kD.

Cross-linking β1 TM1 to TM2

HEK cells were transfected with pWT α and the single mutant L157C(TM2) or the double mutant Y42C(TM1 flank)/L157C(TM2) in the background HIS-FLAG-pWT β1. The β constructs had the additional mutation E13Q. The cells were solubilized with 2 mM *N*-ethylmaleimide and complete protease inhibitors (Roche) in 1% Triton X-100, 200 mM NaCl, 20 mM Tris, and 20 mM imidazole, pH 8.0. The lysate was mixed for 1 h at room temperature with 50 µl of Ni-NTA beads (GE Healthcare), and the beads were washed four times with the same buffer. Proteins were eluted and simultaneously denatured by mixing the beads with 20 mM EDTA, 0.2% SDS, and 20 mM HEPES, pH 7.0; after elution, the eluate was held at 50°C for 20 min. 80 ng Glu-C endoproteinase (Sigma-Aldrich) was added to one half of the eluate, and water was added to the other half; both samples were mixed at room temperature for 18 h. The samples were then split again. 10 mM DTT was added to one half of each sample, and water was added to the other half; all aliquots were held at 50°C for 20 min. Samples were electrophoresed on a 16% Tris-Tricine gel (EC66955; Invitrogen) using Tris/Tricine/SDS buffer (161–0744; Bio-Rad Laboratories), transferred to nitrocellulose, and blotted with HRP-conjugated anti-FLAG antibody (Sigma-Aldrich).

Functional effects of cross-linking

Macroscopic currents were recorded from HEK293 cells in the outside-out patch clamp configuration, as described previously (Liu et al., 2008a,b). For the measurement of conductance as a function of membrane potential (G-V data), macroscopic currents were activated by depolarizing steps from a holding potential of −120 mV and deactivated by repolarization to −120 mV, at which deactivating tail currents were measured. G-V data were fitted with a Boltzmann function. Time constants for activation (step to +80 mV) and deactivation (return to −120 mV) were determined by fitting the macroscopic currents with Clampfit (MDS Analytical Technologies). The bath solution was 150 mM KCl, 5 mM TES, and 1 mM $MgCl_2$, pH 7.5, and the pipette solution was 150 mM KCl, 5 mM TES, 1 mM HEDTA, and 10 µM Ca^{2+}, pH 7.0. The free Ca^{2+} concentration was calculated using the Max Chelator program. Inhibition of BK current by 100 nM iberiotoxin (Tocris Bioscience) was measured 4 min after its addition to the patch.

Structural model of BK α and β1

BK α S1–S6 was built by homology modeling based on the crystal structure of the Kv1.2/Kv2.1 chimera (PDB accession no. 2R9R), using the SWISS-MODEL server (Peitsch, 1995; Arnold et al., 2006; Kiefer et al., 2009). We used PyMol (DeLano, 2002) and Coot (Emsley and Cowtan, 2004) to build S0, TM1, and TM2 as ideal α helices and manually docked them into S1–S6, avoiding steric overlap.

Online supplemental material

Table S1 shows the mean extents of disulfide bond formation between S0 and S1–S4, and Table S2 shows the mean extents of disulfide bond formation between S0 and β1 TM1 and TM2. Fig. S1 shows the cross-linking of two α subunits through the β4 subunit, and Fig. S2 illustrates that the double-Cys mutant β1 Y42C(TM1 flank)/L157C(TM2) coexpressed with either of two single-Cys mutant αs does not form α-β dimers because the intrasubunit TM1 to TM2 cross-link is favored. The online supplemental material is available at http://www.jgp.org/cgi/content/full/jgp.201010417/DC1.

RESULTS

S0 to S1–S4 cross-links

We substituted 64 Cys pairs in FLAG-HRV-pWT α, each with a Cys in S0 and a Cys in one of S1 through S4. These Cys's were in the predicted first turn in the membrane at the extracellular end of the helices (Fig. 1 A). We determined among the BK channels that were trafficked to the cell surface the extent to which each Cys pair formed a disulfide endogenously; i.e., in the absence of added reagents.

FLAG-HRV-pWT α has a predicted molecular mass of 134 kD, and its cleavage with HRV-3C protease produces a 12-kD N-terminal fragment and a 122-kD C-terminal fragment (Fig. 1 B). If there is a disulfide cross-link between S0 and S1–S4, the linked fragments have the same mass and approximately the same electrophoretic mobility as uncleaved α. Reduction of the disulfide with DTT produces the separate N-terminal and C-terminal fragments.

The apparent molecular mass, determined by SDS-PAGE, of pWT-HRV-α, with or without Cys substitution, was ∼125 kD, and that of the C-terminal fragment, identified with an anti–α C-terminal epitope antibody, was ∼110 kD (Fig. 1, C–F). In all cases, after HRV-3C protease and complete DTT reduction, the fraction of total α that ran as an ∼110-kD band was the efficiency of HRV–protease cleavage, which was ∼70% under the conditions used. The extent of intrasubunit S0 to S1–S4 cross-linking was determined from the lane of the unreduced aliquot, corrected by the efficiency of cleavage (see Materials and methods). There was no evidence for inter–α subunit cross-linking, which would have resulted in components with masses that were multiples of ∼125 kD among the uncleaved species.

Cys in the first helical turn of S0 formed disulfide cross-links most readily with Cys in S4, to a lesser extent with Cys in S3, and hardly at all with Cys in S1 and S2 (Figs. 1, C–F, and 2, A–D; Table S1). Taking the mean of the top three extents of cross-linking for each pair of

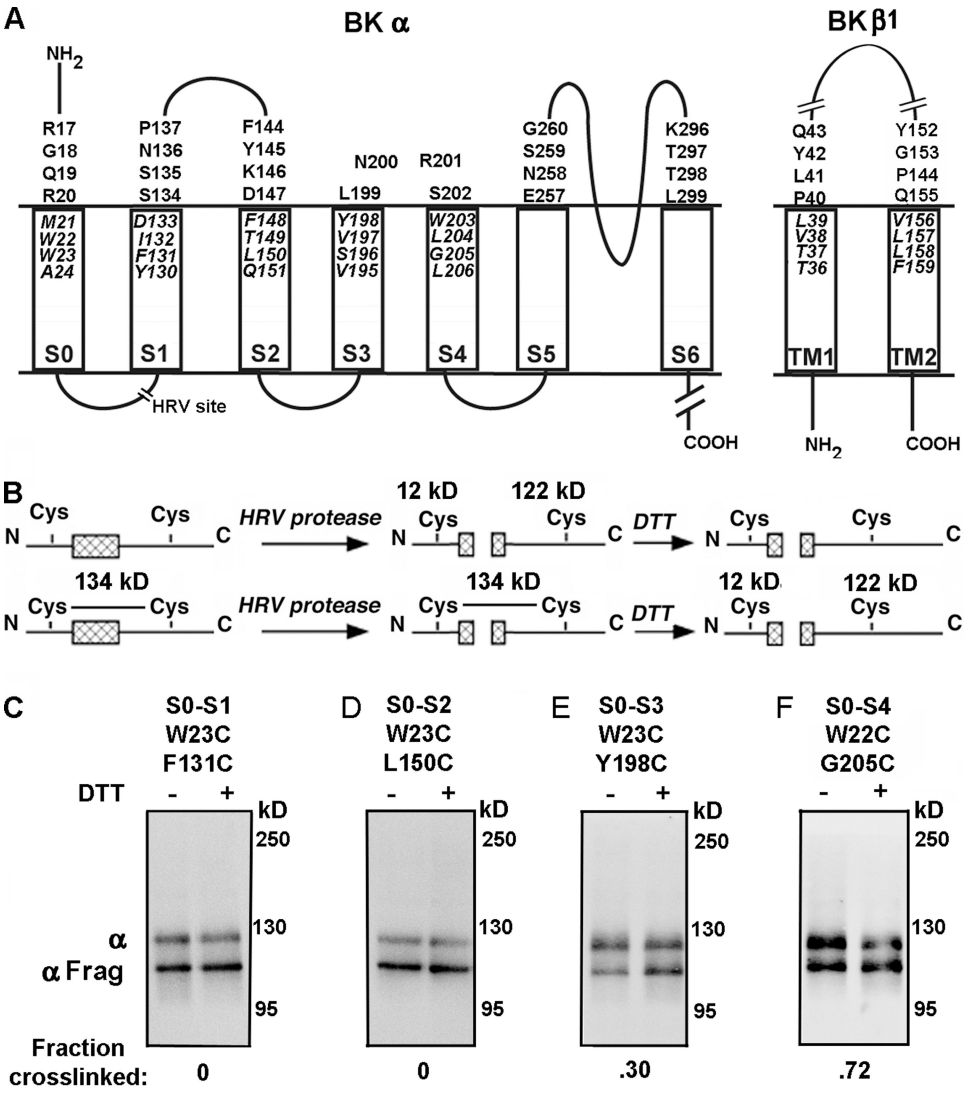

Figure 1. Intra–α subunit disulfide cross-linking from S0 to S1 through S4. (A) Membrane topology of BK α and β1 showing residues mutated to Cys in the predicted first helical turns within the membrane and in the extracellular flanks of the TM helices. The HRV-3C protease cleavage site in the S0–S1 loop is shown as a break. (B) Strategy to determine the extent of disulfide bond formation between S0 and S1 through S4 using HRV-3C protease and DTT. (C–F) The cell surface–expressed double-Cys mutant of α indicated at the top of each immunoblot was treated with HRV-3C protease alone (first lane) or protease followed by DTT (second lane). The immunoblots were developed with an antibody against a C-terminal epitope of α. The extent of cross-linking is indicated under each blot.

TM helices as a measure of the proximity of the segments, we found 7 ± 0% for S0 to S1 (Fig. 2 A), 5 ± 1% for S0 to S2 (Fig. 2 B), 24 ± 7% for S0 to S3 (Fig. 2 C), and 66 ± 6% for S0 to S4 (Fig. 2 D). These results are consistent with S0 in the membrane being closest to S4, less close to S3, and not at all in contact with either S1 or S2. These results are inconsistent with our previous inference that the extracellular end of S0 is between S2 and S3 (Liu et al., 2008a). We now consider an alternative model (Wu et al., 2009) in which S0 is outside of the voltage sensor bundle S1–S4 (Fig. 2 F).

Location of TM1 and TM2 between adjacent voltage sensor domains

Based on disulfide cross-linking between extracellular flanks of the TM helices (Fig. 2 F), we previously inferred that TM2 is close to S0 and that TM1 is close to both S1 and S2 (Liu et al., 2008b). In the membrane, as well, TM2 is close to S0 (Fig. 2 E). 9 of 16 pairs of Cys showed >50% cross-linking, and the average of the top three extents of cross-linking was 80%. In contrast, in the membrane TM1 appeared to have access to, but was not in direct contact with, S1. Of 16 pairs of Cys tested, only 2 showed significant cross-linking: V38C(TM1) cross-linked to I132C(S1) to the extent of 28%, and T36C(TM1) cross-linked to I132C(S1) to the extent of 13% (Table S2). There was even less cross-linking in the membrane between TM1 and S2. Even though the TM1 flank is close to the flanks of S1 and S2, the helices themselves likely diverge in the membrane.

If TM1 and TM2 from a single β1 were positioned between adjacent voltage sensors (Fig. 2 F), it should be possible for us to cross-link two α subunits through one β subunit. We tested this with the double-Cys–substituted α W23C(S0)/F144C(S2 flank) and the double-Cys–substituted β1 Y42C(TM1 flank)/L157C(TM2). These residues were chosen because α W23C(S0) and β1 L157C(TM2), in the membrane, were ∼70% cross-linked

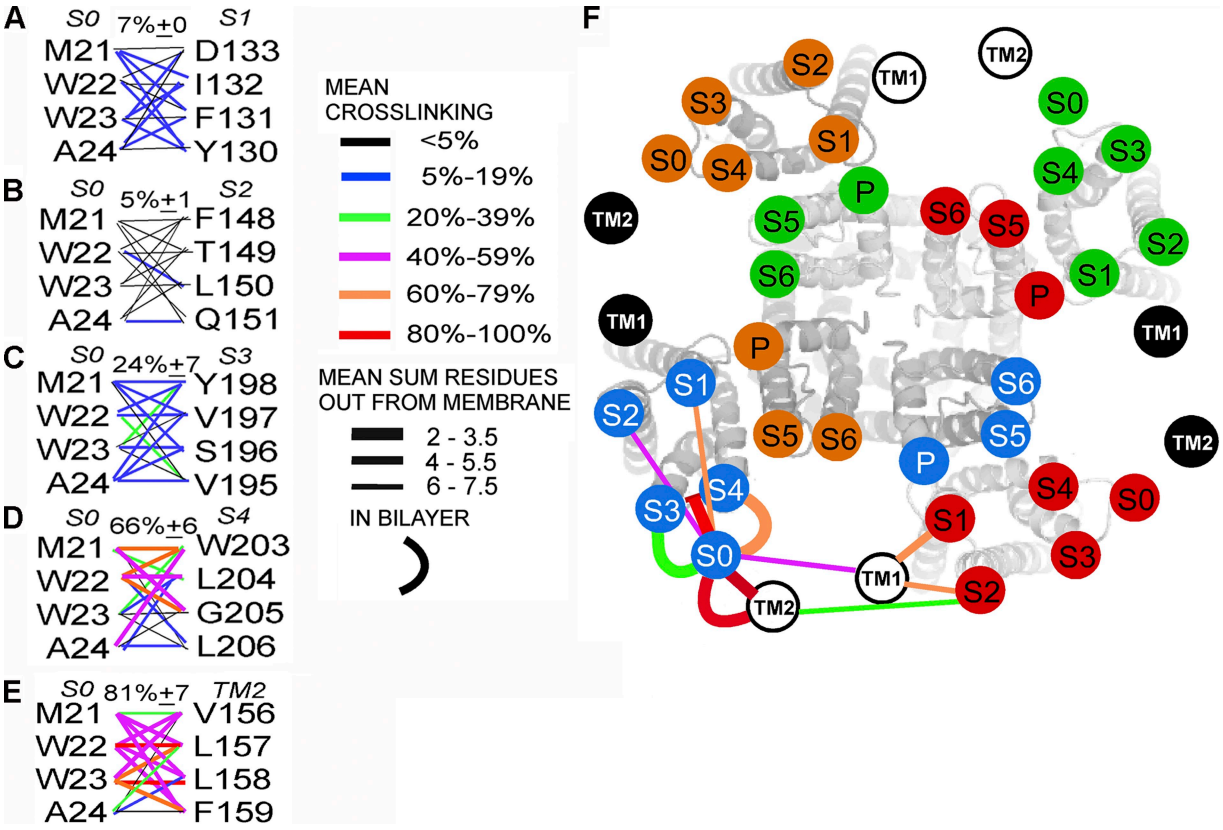

Figure 2. Extents of endogenous disulfide bond formation between S0 and S1 through S4 and between S0 and TM2. (A–E) In the left column, the four residues substituted by Cys in the first helical turn in the membrane of S0 are shown, and the four residues substituted in (A) S1, (B) S2, (C) S3, (D) S4, and (E) TM2 are in the right column. The mean extents of disulfide bond formation between Cys are represented by connecting lines color-coded according to the legend. The means of the top three extents of cross-linking are shown above each set of lines. (F) Face-on view of the Kv1.2/Kv2.1 chimera S1–S6 with superimposed, labeled circles, uniquely colored for each subunit, representing the approximate locations of the extracellular ends of BK α S1–S6. Circles representing the extracellular ends of BK α S0 and of β1 TM1 and TM2 are located relative to S1–S6, based on the extents of cross-linking between Cys in the extracellular flanks (straight lines) and on the extents of cross-linking between Cys in the membrane (curved lines). The lines are color-coded for the mean extent of cross-linking (mean of the top three pairs) and coded by line thickness for the extracellular cross-links by the mean sum of the number of residues that the two Cys's are out from the membrane. The closer the cross-links between the extracellular flanks are to the membrane, the thicker the line.

(Fig. 3 A), and α F144C(S2 flank) and β1 Y42C(TM1 flank) were also ∼70% cross-linked (Fig. 3 B) (Liu et al., 2008b). When α W23C(S0)/F144C(S2 flank) and β1 Y42C(TM1 flank)/L157C(TM2) were coexpressed, a component of apparent mass of ∼340 kD appeared (Fig. 3 C, first lane). This band was not present after treatment of the intact cells with DTT (Fig. 3 C, second lane) and was restored after subsequent treatment of the cells with the doubly charged, membrane-impermeant oxidizing agent quaternary piperazinium diamide (QPD) (Fig. 3 C, third lane) (Liu et al., 2008a). The apparent molecular mass is consistent with the band containing at least one of the cross-linked species α-β-α (predicted molecular mass of 290 kD), α-β-α-β (predicted molecular mass of 320 kD), or β-α-β-α-β (predicted molecular mass of 350 kD). In each of these, two αs are cross-linked via one β. Identical results were obtained with another β type, FLAG-β4 L44C(TM1)/H172C(TM2) coexpressed with α W23C(S0)/F144C(S2 flank) (Fig. S1).

To determine whether the ∼340-kD component, visualized with anti-α antibody, also contained β1, we coexpressed the double-Cys–substituted pWT α (no FLAG tag) W23C(S0)/F144C(S2 flank) with the double-Cys–substituted, FLAG-tagged β1 Y42C(TM1 flank)/L157C(TM2). The transfected cells were surface labeled with sulfoNHS-LC-biotin and lysed. A portion of the lysate was directly denatured in SDS and electrophoresed (Fig. 3 D), and the rest was first mixed with anti–FLAG antibody Sepharose to capture components containing FLAG-tagged β1, which were eluted with FLAG peptide (Fig. 3 E). In parallel controls, double-Cys–substituted α was coexpressed without FLAG-β1, with FLAG-β1 without substituted Cys, with single-Cys–substituted β1 Y42C(TM1 flank), and with single-Cys–substituted β1 L157C(TM2).

In the absence of FLAG-β1, α was predominantly monomeric in the lysate (Fig. 3 D, lane 1) and absent in the eluate from anti–FLAG Sepharose (Fig. 3 E, lane 1). Similarly, after coexpression of the double-Cys–substituted α W23C(S0)/F144C(S2 flank) with FLAG-β1 (no Cys substitution), monomeric α appeared in the lysate (Fig. 3 D, lane 2), but very little in the eluate from anti–FLAG Sepharose (Fig. 3 E, lane 2). Coexpression of the double-Cys–substituted α with single-Cys–substituted FLAG-β1, either Y42C(TM1 flank) or L157C(TM2), resulted in α-β1 dimer in both the lysate and the eluate from anti–FLAG Sepharose (Fig. 3, D and E, lanes 3 and 4). Finally, coexpression of the double-Cys–substituted α W23C(S0)/F144C(S2 flank) with the double-Cys–substituted FLAG-β1 Y42C(TM1 flank)/L157C(TM2) resulted in an ∼340-kD band both in the lysate (Fig. 3 D, lane 5) and in the eluate from anti–FLAG Sepharose (Fig. 3 E, lane 5). We conclude that α was not captured by the anti–FLAG Sepharose if it was not cross-linked to FLAG-β1, and that the ∼340-kD band contained both α and β1.

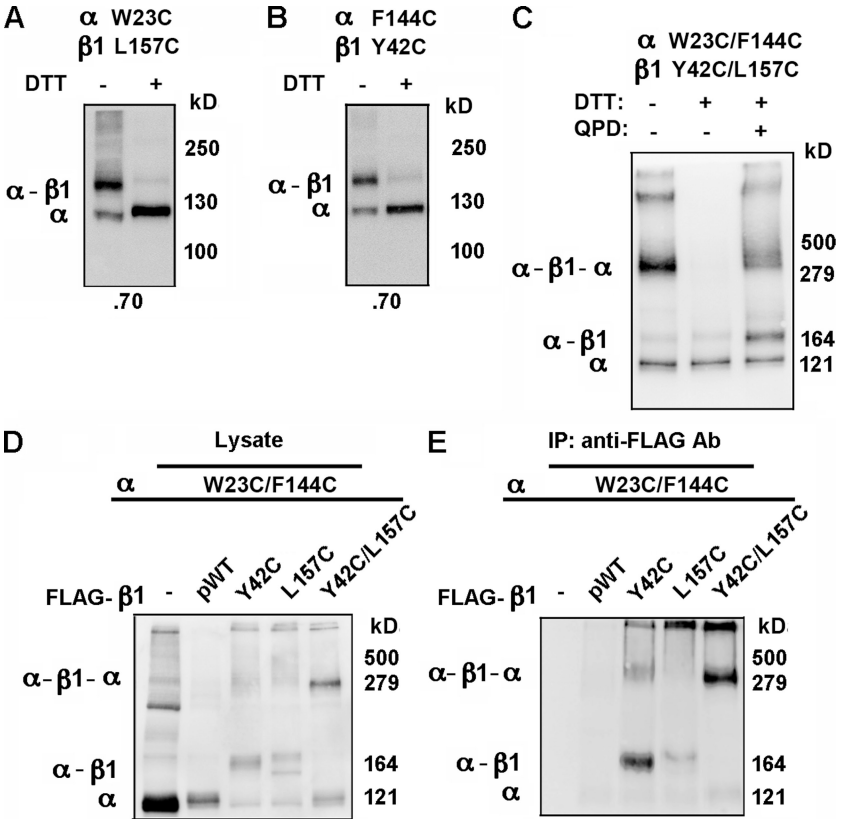

Figure 3. Cross-linking of two α subunits through one β1 subunit. (A and B) The single-Cys mutants of FLAG-pWT α and pWT β1 were coexpressed, and the extent of α-β1 cross-linking (indicated at the bottom) was determined. The effect of DTT reduction of the samples is shown in the second lane. (C) Cells expressing the double-Cys mutants of FLAG-HRV-pWT α and pWT β1 were either untreated (lane 1), treated with 20 mM DTT (lane 2), or treated with 20 mM DTT and then, after washing, with 40 µM quaternary piperazinium diamide (QPD; lane 3). (D) Whole lysate of surface-labeled cells expressing the indicated α and β constructs. (E) FLAG-pWT β1 and its Cys mutants in the same cell extracts as in D were captured by anti-FLAG antibody conjugated to Sepharose (Sigma-Aldrich) and were eluted with FLAG peptide. Biotinylated complexes in this extract were captured on Neutravidin beads, released in SDS, and electrophoresed, immunoblotted, and visualized with anti-α antibody and HRP-tagged secondary antibody.

Cross-linking of β TM1 and TM2

In the new model (Fig. 2 F), in contrast to our original model (Liu et al., 2008b), TM1 and TM2 are adjacent. In that case, appropriately located Cys in TM1 and in TM2 should be capable of forming a disulfide. That Y42C(TM1 flank) and L157C(TM2) might be such a pair was suggested by the observation that neither single-Cys–substituted α W23C(S0) or α F144C(S2 flank) formed a cross-linked dimer with the double-Cys–substituted β1 Y42C(TM1 flank)/L157C(TM2) (Fig. S2), even though the single-Cys mutant α W23C(S0) readily cross-linked to β1 L157C(TM2) (Fig. 3 A), and α F144C(S2 flank) readily cross-linked to β1 Y42C(TM1 flank) (Fig. 3 B). It appeared that if one of the two β1 Cys's did not have a partner in α, the β1 Cys's preferred to cross-link to each other. This preference argues that the component with an apparent mass of ∼340 kD is α-β-α and not a species that has an additional β at either end cross-linked to just one α.

To test for cross-linking between these two β1 Cys's directly, we used a β1 construct in which exhaustive proteolysis by GluC endoproteinase produces a unique N-terminal fragment that includes TM1 and a unique C-terminal fragment that includes TM2 (Fig. 4 A). The cleavage site closest to the N terminus is Glu50, and the cleavage site closest to the C terminus is Glu143. The Cys substituted for Tyr42 is in the flank of TM1, and the Cys substituted for Leu157 is in TM2. The four native Cys's that form two disulfides in the β1 loop and the two *N*-glycosylated sites are between Glu50 and Glu143. GluC generates an N terminal fragment (Frag A) of predicted mass of 7.7 kD and a C-terminal fragment (Frag B) of predicted mass of 5.4 kD. If, however, Cys42 is cross-linked to Cys157, Frag A will be disulfide cross-linked to Frag B, with a combined mass of 13.1 kD.

The double-Cys mutant β1 Y42C(TM1 flank)/L157C (TM2) was made in the background E13Q, C18A, and C26A, and a 6-His tag and a FLAG tag were added to the N terminus of β1. In addition, as a control, the single-Cys mutant β1 L157C(TM2) was produced in the same background. These constructs were coexpressed with pWT α. The cells were lysed, and β1 was captured on Ni-NTA Sepharose, eluted in 20 mM EDTA, denatured in SDS, and cleaved overnight with GluC. Unreduced and reduced aliquots were electrophoresed and blotted, and the fragments containing the N terminus were visualized with anti-FLAG antibody conjugated to HRP.

In the absence of GluC, the coexpressed single-Cys mutant β1 had an apparent mass of ∼33 kD, whether or not the sample was reduced with DTT (Fig. 4 B). After cleavage with GluC, the only FLAG-containing fragment had an apparent mass of ∼8.3 kD, close to that predicted for the N-terminal fragment containing TM1. In the absence of GluC, whether or not the sample was reduced with DTT, the double-Cys mutant β1 also had an apparent mass of ∼33 kD (Fig. 4 C). After GluC, there was only one component containing the N-terminal FLAG tag, and it had an apparent mass of ∼13 kD, consistent with the predicted mass of cross-linked Frag A and Frag B. After reduction with DTT, there was again only one FLAG-tagged fragment. It had an apparent mass of ∼8.3 kD and corresponded to Frag A. Because after GluC, but before reduction, there is no other FLAG-tagged component, all of β1 in the cell lysate is cross-linked between Y42C(TM1 flank) and L157C(TM2). This result is consistent with close contact between TM1 and TM2.

Function of cross-linked α and β1

The question of whether the cross-linking of TM1 to TM2 and the cross-linking of two αs through one β occur

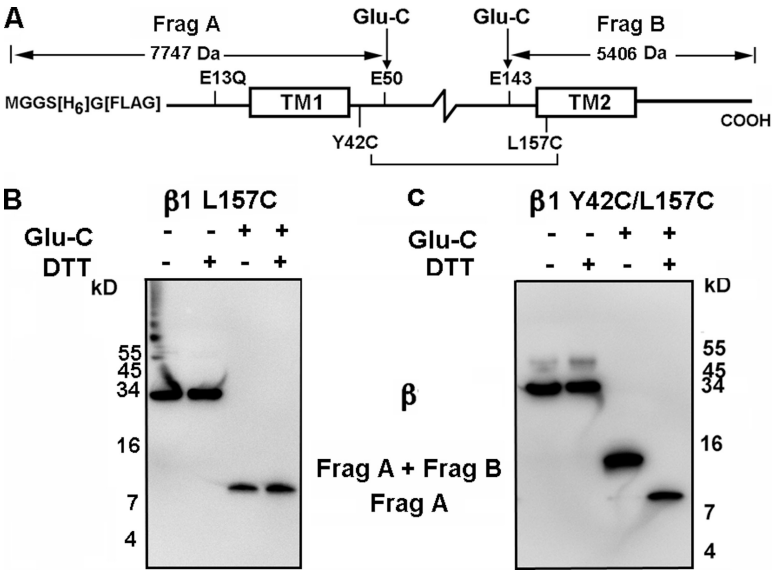

Figure 4. Cross-linking TM1 to TM2. (A) HIS-FLAG-pWT β1 and the detection of cross-linking. Complete cleavage by GluC endoproteinase yields an N-terminal fragment, which includes TM1, with a mass of 7.7 kD, and a C-terminal fragment, which includes TM2, with a mass of 5.4 kD. If these fragments were cross-linked between Y42C(TM1 flank) and L157C(TM2), the combined fragments detected with anti-FLAG antibody would have a mass of 13.1 kD. After DTT reduction, only the 7.7-kD N-terminal fragment would be detected with anti-FLAG antibody. (B) HIS-FLAG-pWT β1 L157C(TM2) and pWT α were coexpressed, extracted, bound to Ni-NTA agarose beads, eluted, and treated with GluC endoproteinase and DTT. (C) Double-Cys mutant HIS-FLAG-pWT β1 Y42C(TM1 flank)/L157C(TM2) coexpressed with pWT α and treated as in B.

in near-native structures of α and β1 can be answered in part by determining the functional properties of the cross-linked subunits. β1 normally slows activation and deactivation of the channel, shifts the G-V curve for opening to the left (in the presence of Ca^{2+}), and protects against inhibition by iberiotoxin (Meera et al., 2000; Lippiat et al., 2003). These effects are shown by comparing the properties of the channel formed by FLAG-HRV-pWT α alone (Fig. 5, A, F, and K–N) and of the channel formed by FLAG-HRV-pWT α plus pWT β1 (Fig. 5, B, G, and K–N). The double-Cys–substituted β1 Y42C(TM1 flank)/L157C(TM2) also slows activation and deactivation of pWT α (Fig. 5, C, L, and M), protects against block by iberiotoxin (Fig. 5, H and K), and shifts the G-V curve of pWT α to the left, albeit not as much as pWT β1 (Fig. 5 N). Because all the expressed double-Cys–substituted β1 is cross-linked between TM1 and TM2, and because the channel is modulated, cross-linked β1 associates with pWT α and is functional.

It is evident from the immunoblot assay of cross-linking that the double-Cys–substituted α W23C(S0)/F144C(S2 flank) associates with the double-Cys mutant β1 Y42C(TM1 flank)/L157C(TM2), and that the subunits on the cell surface are almost completely cross-linked (Fig. 3, C and E). Moreover, in this cross-linked complex, β1 still modulates α. Compared with the channel

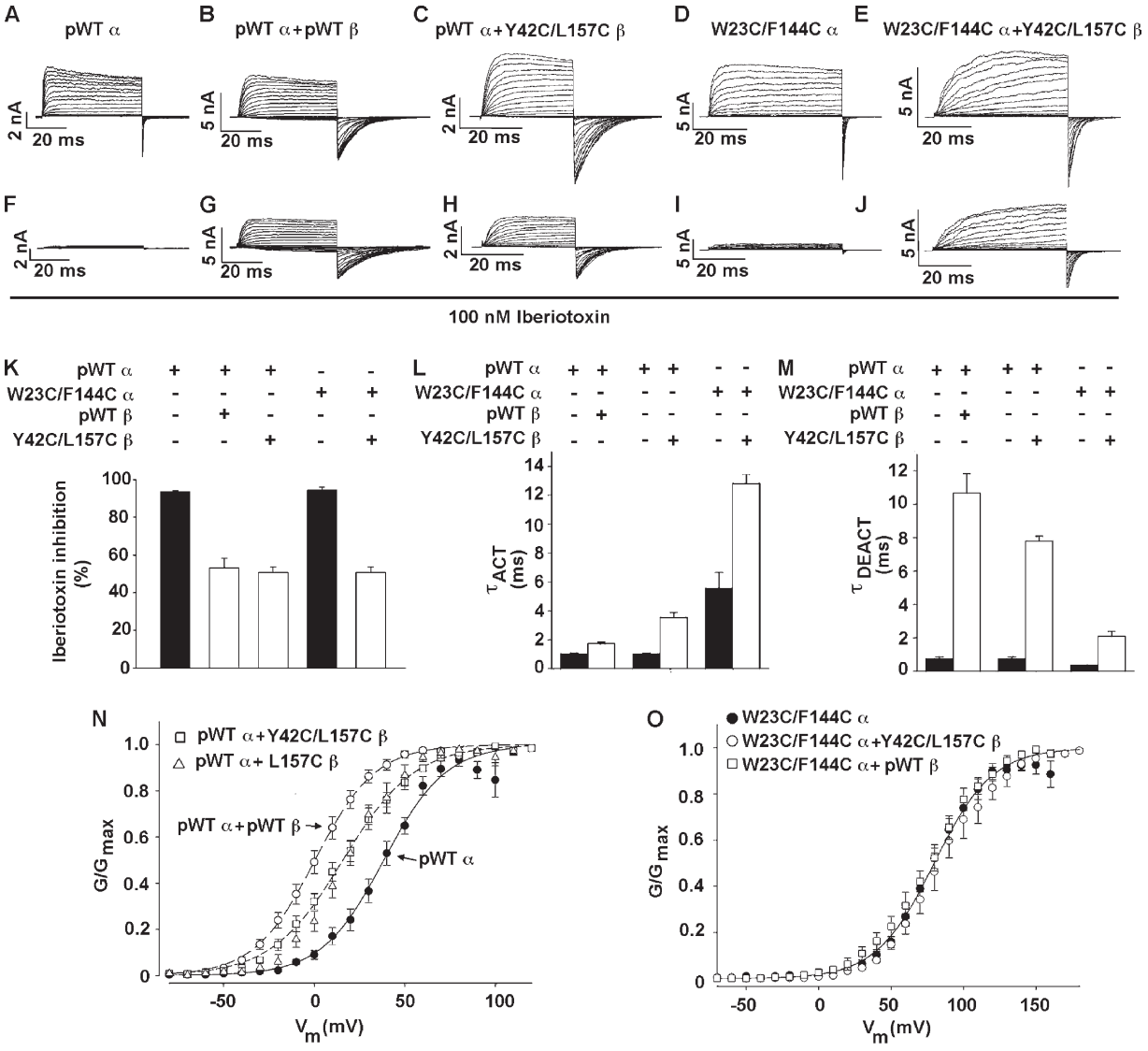

Figure 5. Functional effects of disulfide cross-links. (A–E) Currents due to the indicated subunit combinations in response to step depolarizations from −40 to +140 mV, and then back to −80 mV. The recordings were made in outside-out macropatches with 10 μM Ca^{2+} inside the pipette. (F–J) Currents obtained with the same macropatches as above 4 min after the addition of 100 nM iberiotoxin to the perfusion solution. (K) Mean and SD (n = 4–5) of inhibition after 4-min exposure to 100 nM iberiotoxin. (L) Mean time constants for activation (τ_{ACT}) (n = 4–5) for the indicated subunit combinations. (M) Mean time constants for deactivation (τ_{DEACT}) (n = 4−5). (N and O) Normalized G-V curves with 10 μM Ca^{2+} inside the pipette for the indicated subunit combinations. Fits of a Boltzmann equation were to the means and SD (n = 4–10) of normalized conductances from separate patches.

formed by α W23C(S0)/F144C(S2 flank) alone, the channel formed by α W23C(S0)/F144C(S2 flank) and β1 Y42C(TM1 flank)/L157C(TM2) activates and deactivates more slowly (Fig. 5, D, E, L, and M). Furthermore, β1 Y42C(TM1 flank)/L157C(TM2) protects the channel against iberiotoxin (Fig. 5, J and K). Neither β1 Y42C(TM1 flank)/L157C(TM2) nor pWT β1, however, shifts the G-V curve of α W23C(S0)/F144C(S2 flank), which is shifted 50 mV to the right of the G-V curve of the channel formed by pWT α (Fig. 5 O). Thus, it is not the cross-links to the double-Cys–substituted β1 that prevent the leftward shift in the G-V curve of the double-Cys–substituted α, but rather the mutations in α per se. The G-V curve of the channel formed by α with just one of these mutations, W23C(S0), was also not shifted by pWT β1 (not depicted), pointing to the possible involvement in the leftward shift in the G-V curve of the interface between α S0 and β1 TM2 in the neighborhood of W23.

DISCUSSION

Proximity by disulfide cross-linking

Compared with extracellular Cys, Cys in the membrane domain will, on average, ionize less and be less accessible to oxidizing agents and to enzymes. Nevertheless, as previously reported for extracellular Cys (Liu et al., 2008a,b; Wu et al., 2009), there was considerable disulfide formation in some of the pairs of Cys's in the membrane, even in the absence of added oxidizing agents. Among the possible mechanisms for endogenous disulfide bond formation (i.e., in the absence of exogenous reagents), we previously argued (Liu et al., 2008a) that catalytic formation by a protein disulfide isomerase (PDI) in the ER (Wilkinson and Gilbert, 2004) was a more likely mechanism than was spontaneous oxidation by dissolved O_2 or oxidation by secreted enzymes (Jiang et al., 1999; Becker et al., 2006). We surmised that the steady-state extent of the cross-linking of two Cys's reflects the relative stability of the structure constrained by their cross-linking compared with the stability of the disulfide in the catalytic site of the PDI (Liu et al., 2008a). A major determinant of the stability of a protein disulfide is the proximity of the Cys in the native structure. We infer the relative proximities of four-residue segments of helices and their flanks by determining the extents of cross-linking of at least 16 pairs of Cys's and taking the average of the top three extents of cross-linking as an indicator of relative proximity. By this criterion, at their extracellular ends in the membrane, TM2 and S4 are closest to S0, S3 is not as close to S0, and S1 and S2 are not close at all. Only 2 of 16 Cys pairs in TM1 and S1 cross-link significantly, and none of the pairs in TM1 and S2 cross-link. Therefore, despite extensive cross-linking between the flank of TM1 and the flanks of S1 and S2, these helices likely diverge in the membrane.

A question is whether or not cross-linking reflects the distances in a native structure or in some nonnative structure. We determined the extents of disulfide formation in channels that were expressed on the cell surface. Transport to the cell surface is selective for well-folded proteins. In addition, those disulfide cross-linked channels that were tested were functional, albeit in some cases with perturbed characteristics. Although these cross-linked mutants cannot be completely native, their structures are close enough to native to be transported to the cell surface and to function as BK channels (e.g., Fig. 5).

Space-filling model

A three-dimensional model of BK α S1 through S6 (Fig. 6 A) was generated by homology modeling based on the structure of the Kv1.2/Kv2.1 chimera (Long et al., 2005). We added BK α S0 and β1 TM1 and TM2 as standard α helices. We avoided steric clashes but did not minimize the energy of the structure. Our placement of S0, TM1, and TM2 was consistent with the current cross-linking results in the membrane and the previous cross-linking between the extracellular flanks (Fig. 2 F). Finally, the model is consistent with the cross-linking of TM1 to TM2 and the cross-linking of two αs through one β, S0 to TM2 and TM1 to S2. In particular, the following paired residues substituted by Cys that readily formed disulfides were positioned within striking distance of each other: S0 W22 and S4 W203, S0 W22 and S4 G205, and S0 W23 and TM2 L157 (Fig. 6 B). The model shows that locating the three helices, S0, TM2, and TM1, in the gap between adjacent voltage sensor domains is spatially feasible.

In the helical turns that extensively cross-link to each other, S0 to S4 and S0 to TM2, there is significant cross-linking of Cys around nearly complete turns of the helices (Fig. 2, D and E, and Tables S1 and S2). Either the orientation of these helices around their long axes or their local secondary structure fluctuates. It is possible that the first helical turns unwind during oxidation by a PDI, which has chaperone-like activity. Some of these cross-links must distort the native structure, but nevertheless the channels are trafficked to the cell surface and function.

The previously observed cross-linking of the S0 flank to the flanks of S1 and S2 of the same subunit requires that this flank cross over the four-residue S3–S4 loop and reach the flanks of S1 and S2. The disulfides are formed between Cys substituted three or four residues out from the membrane on each of the flanks (Liu et al., 2008a) with a combined reach of the backbone plus the two Cys side chains of ∼26 Å. The distance in a space-filling model (Fig. 6) from the extracellular end of S0 to the extracellular end of S1 is 16 Å and to the extracellular end of S2 is 23 Å. We showed previously that in wild-type (WT) α, Cys14, seven residues N-terminal to S0,

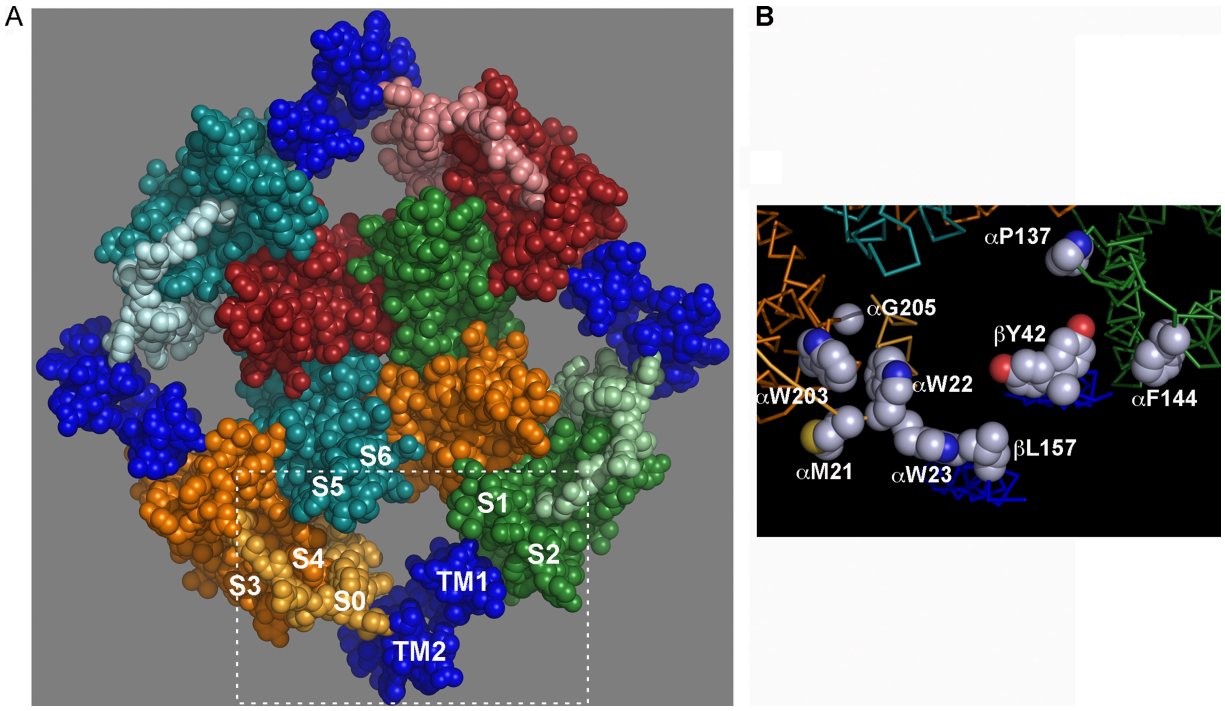

Figure 6. Model of BK α and β1. BK α S1 through S6 was built by homology modeling (see Materials and methods) based on the crystal structure of the Kv1.2/Kv2.1 chimera (PDB accession no. 2R9R). S1–S6 of each subunit has a unique color, and the color of S0 is a lighter shade of the S1–S6 color. β1 TM1 and TM2 are dark blue, with TM2 next to S0. Residues 16–20 of the extracellular N-terminal segment preceding S0 were modeled as a random coil, crossing over the S3–S4 loop. (B) The boxed in area in A, showing residue side chains, which when substituted by Cys, readily formed disulfide cross-links, including both M21 and W22 in S0 and both W203 and G205 in S4, W23 in S0, β1 L157 in TM2, β1 Y42 in the TM1 flank (two rotamers are shown), α P137 in the S1 flank, and F144 in the S2 flank. Atoms are in full CPK volume. Hydrogens are not shown. Side chain carbons are gray, oxygens are red, and nitrogens are blue.

and Cys141, in the middle of the 14-residue S1–S2 loop, form a disulfide (Liu et al., 2008a). Therefore, in WT α, the extracellular, N-terminal tail of α, including the S0 flank, normally runs in the direction of the S1–S2 loop.

Functional implications of the positions of S0, TM1, and TM2

Compared with other voltage-gated K^+ channels, the V_{50} for gating charge movement of the voltage sensors of BK α alone is shifted to much more positive voltages, and even though the magnitude of the gating charge per voltage sensor is smaller (Stefani et al., 1997; Horrigan and Aldrich, 1999; Bao and Cox, 2005), the electrostatic energy needed to activate each voltage sensor is greater (Liu et al., 2008a). We speculated that the association of S0, unique to BK α, with the S1–S4 voltage sensor domain contributes to the stabilization of the closed state relative to the open state (Liu et al., 2008a). We now find that S0 in the membrane, at least at its extracellular end, is most closely associated with S4, and this association is likely to play a role in the difference in free energy between the activated and deactivated states of the individual voltage sensor domains. In addition, S0 forms a major contact with TM2 of β1 (Liu et al., 2008b) and β4 (Wu et al., 2009).

The BK channel is a soft machine in which the moving parts, the voltage-sensing domains and the gate, are linked to each other probabilistically (Cox et al., 1997; Horrigan et al., 1999; Horrigan and Aldrich, 1999, 2002; Niu et al., 2004; Horrigan and Hoshi, 2008). The changing contacts of these moving parts of α, with different free energies of association with β, are the mechanism for β's modulation of α. We have now shown that β1 TM1 and TM2 are contiguous and positioned with TM2 next to S0 of one voltage-sensing domain and TM1 within reach of S1 and S2 of the adjacent voltage-sensing domain. Although these contacts provide opportunities for the modulation of the voltage dependence of voltage sensor movement and for the slowing of channel opening and closing, at least at their extracellular ends, S4, S0, and TM2 seem not to move much relative to one another during activation and deactivation. Nearly complete cross-linking of L199C in the S3–S4 linker to R20C in the S0 flank, R201C in the S3–S4 linker to R17C or G18C in the S0 flank, and of R17C in the S0 flank to Q155C in the TM2 flank had almost no effect on V_{50} for opening or on the kinetics of activation and deactivation compared with WT α-β1 (Liu et al., 2008a,b) . We now find that cross-linking of two αs through one β1 does prevent the leftward shift in V_{50} due to β1, although this appears to be due almost entirely

to one of the four mutations, W23C(S0). Despite the double cross-links, however, β1 still slows both activation and deactivation. We conclude that the extracellular ends of S0, S2, TM1, and TM2 do not undergo large relative motions during activation, deactivation, and gating. Perturbations of their structures and interactions and constraints on their motion have slight to moderate effects on function but do not disrupt channel function. Of course, more of their surfaces of interaction in the membrane domain remain to be explored.

In addition to the contacts between the extracellular ends of the TM helices, the 116-residue extracellular loop between β1 TM1 and TM2 reaches close to the central pore (Knaus et al., 1994a; Hanner et al., 1997), where it protects against block by iberiotoxin and charybdotoxin (Knaus et al., 1994a; Hanner et al., 1997; Meera et al., 2000; Lippiat et al., 2003). The effects of two human mutations imply that contact between the β1 loop and α also affects the free energy difference between the closed and open states of the channel: β1 E65K (Fernández-Fernández et al., 2004) shifts the G-V curve to the left and protects against diastolic hypertension, and β1 R140W (Seibold et al., 2008) shifts the G-V curve to the right and is associated with an increased risk for airway obstruction and asthma morbidity. The intracellular N-terminal and C-terminal tails of β are also likely to have roles in the modulation of α (Wang et al., 2006). In β2 and β3a, the relatively long N-terminal tail inactivates the channel via an inactivation ball (Wallner et al., 1999; Uebele et al., 2000; Xia et al., 2000; Wang et al., 2002). The positions of the loop and the tails, as well as possible cross-talk between them, depend on TM1 and TM2.

The exact path of the loop is not known, but given the positions of TM1 and TM2 (Fig. 6 A), it is likely that the β loop passes over at least one of the pore-forming helices of a third α subunit, so that each β subunit may interact with three different α subunits. Among these interactions, it is the interaction of TM2 with S0, and thereby with the voltage sensor domain, that is likely to play a major role in the stabilization of the activated state of the voltage sensor by β1 (Bao and Cox, 2005).

This work was supported in part by National Institutes of Health (NIH) research grant awards P01 HL081172 and R01 HL68093 from National Heart, Lung and Blood Institute and R01 NS054946 from National Institute of Neurological Disorders and Stroke, and the Arlene and Arnold Goldstein Family Foundation. S.O. Marx is an Established Investigator of the American Hearth Association (AHA). G. Liu is supported by an AHA Scientist-Development Award. R.S. Wu was supported by an NIH T32 HL07854 and Future Leaders in CV Medical Research award from Schering-Plough. N. Chudasama was supported by the Doris Duke Clinical Research Fellowship Program.

Christopher Miller served as editor.

Submitted: 11 February 2010
Accepted: 29 March 2010

REFERENCES

Arnold, K., L. Bordoli, J. Kopp, and T. Schwede. 2006. The SWISS-MODEL workspace: a web-based environment for protein structure homology modelling. *Bioinformatics.* 22:195–201. doi:10.1093/bioinformatics/bti770

Bao, L., and D.H. Cox. 2005. Gating and ionic currents reveal how the BK_{Ca} channel's Ca^{2+} sensitivity is enhanced by its β1 subunit. *J. Gen. Physiol.* 126:393–412. doi:10.1085/jgp.200509346

Becker, L., M.E. Nesheim, and M.L. Koschinsky. 2006. Catalysis of covalent Lp(a) assembly: evidence for an extracellular enzyme activity that enhances disulfide bond formation. *Biochemistry.* 45:9919–9928. doi:10.1021/bi060283t

Brenner, R., T.J. Jegla, A. Wickenden, Y. Liu, and R.W. Aldrich. 2000. Cloning and functional characterization of novel large conductance calcium-activated potassium channel beta subunits, hKCNMB3 and hKCNMB4. *J. Biol. Chem.* 275:6453–6461. doi:10.1074/jbc.275.9.6453

Butler, A., S. Tsunoda, D.P. McCobb, A. Wei, and L. Salkoff. 1993. mSlo, a complex mouse gene encoding "maxi" calcium-activated potassium channels. *Science.* 261:221–224. doi:10.1126/science.7687074

Cox, D.H., J. Cui, and R.W. Aldrich. 1997. Allosteric gating of a large conductance Ca-activated K^+ channel. *J. Gen. Physiol.* 110:257–281. doi:10.1085/jgp.110.3.257

DeLano, W.L. 2002. PyMOL Molecular Viewer. http://www.pymol.org (accessed March 31, 2010).

Emsley, P., and K. Cowtan. 2004. Coot: model-building tools for molecular graphics. *Acta Crystallogr. D Biol. Crystallogr.* 60:2126–2132. doi:10.1107/S0907444904019158

Fernández-Fernández, J.M., M. Tomás, E. Vázquez, P. Orio, R. Latorre, M. Sentí, J. Marrugat, and M.A. Valverde. 2004. Gain-of-function mutation in the KCNMB1 potassium channel subunit is associated with low prevalence of diastolic hypertension. *J. Clin. Invest.* 113:1032–1039.

Hanner, M., W.A. Schmalhofer, P. Munujos, H.G. Knaus, G.J. Kaczorowski, and M.L. Garcia. 1997. The beta subunit of the high-conductance calcium-activated potassium channel contributes to the high-affinity receptor for charybdotoxin. *Proc. Natl. Acad. Sci. USA.* 94:2853–2858. doi:10.1073/pnas.94.7.2853

Horrigan, F.T., and R.W. Aldrich. 1999. Allosteric voltage gating of potassium channels II. Mslo channel gating charge movement in the absence of Ca^{2+}. *J. Gen. Physiol.* 114:305–336. doi:10.1085/jgp.114.2.305

Horrigan, F.T., and R.W. Aldrich. 2002. Coupling between voltage sensor activation, Ca^{2+} binding and channel opening in large conductance (BK) potassium channels. *J. Gen. Physiol.* 120:267–305. doi:10.1085/jgp.20028605

Horrigan, F.T., and T. Hoshi. 2008. Integration of an electric-metal sensory experience in the Slo1 BK channel. *Nat. Struct. Mol. Biol.* 15:1130–1132. doi:10.1038/nsmb1108-1130

Horrigan, F.T., J. Cui, and R.W. Aldrich. 1999. Allosteric voltage gating of potassium channels I. Mslo ionic currents in the absence of Ca^{2+}. *J. Gen. Physiol.* 114:277–304. doi:10.1085/jgp.114.2.277

Jiang, X.M., M. Fitzgerald, C.M. Grant, and P.J. Hogg. 1999. Redox control of exofacial protein thiols/disulfides by protein disulfide isomerase. *J. Biol. Chem.* 274:2416–2423. doi:10.1074/jbc.274.4.2416

Kiefer, F., K. Arnold, M. Künzli, L. Bordoli, and T. Schwede. 2009. The SWISS-MODEL repository and associated resources. *Nucleic Acids Res.* 37:D387–D392. doi:10.1093/nar/gkn750

Knaus, H.G., A. Eberhart, G.J. Kaczorowski, and M.L. Garcia. 1994a. Covalent attachment of charybdotoxin to the beta-subunit of the high conductance Ca(2+)-activated K+ channel. Identification of the site of incorporation and implications for channel topology. *J. Biol. Chem.* 269:23336–23341.

Knaus, H.G., K. Folander, M. Garcia-Calvo, M.L. Garcia, G.J. Kaczorowski, M. Smith, and R. Swanson. 1994b. Primary sequence

and immunological characterization of beta-subunit of high conductance Ca(2+)-activated K+ channel from smooth muscle. *J. Biol. Chem.* 269:17274–17278.

Lippiat, J.D., N.B. Standen, I.D. Harrow, S.C. Phillips, and N.W. Davies. 2003. Properties of BK(Ca) channels formed by bicistronic expression of hSloalpha and beta1-4 subunits in HEK293 cells. *J. Membr. Biol.* 192:141–148. doi:10.1007/s00232-002-1070-0

Liu, G., S.I. Zakharov, L. Yang, S.X. Deng, D.W. Landry, A. Karlin, and S.O. Marx. 2008a. Position and role of the BK channel α subunit S0 helix inferred from disulfide crosslinking. *J. Gen. Physiol.* 131:537–548. doi:10.1085/jgp.200809968

Liu, G., S.I. Zakharov, L. Yang, R.S. Wu, S.X. Deng, D.W. Landry, A. Karlin, and S.O. Marx. 2008b. Locations of the beta1 transmembrane helices in the BK potassium channel. *Proc. Natl. Acad. Sci. USA.* 105:10727–10732. doi:10.1073/pnas.0805212105

Long, S.B., E.B. Campbell, and R. Mackinnon. 2005. Crystal structure of a mammalian voltage-dependent Shaker family K+ channel. *Science.* 309:897–903. doi:10.1126/science.1116269

Meera, P., M. Wallner, and L. Toro. 2000. A neuronal beta subunit (KCNMB4) makes the large conductance, voltage- and Ca2+-activated K+ channel resistant to charybdotoxin and iberiotoxin. *Proc. Natl. Acad. Sci. USA.* 97:5562–5567. doi:10.1073/pnas.100118597

Niu, X., X. Qian, and K.L. Magleby. 2004. Linker-gating ring complex as passive spring and Ca(2+)-dependent machine for a voltage- and Ca(2+)-activated potassium channel. *Neuron.* 42:745–756. doi:10.1016/j.neuron.2004.05.001

Peitsch, M.C. 1995. Protein modeling by email. *Nat. Biotechnol.* 13:658–660. doi:10.1038/nbt0795-658

Seibold, M.A., B. Wang, C. Eng, G. Kumar, K.B. Beckman, S. Sen, S. Choudhry, K. Meade, M. Lenoir, H.G. Watson, et al. 2008. An african-specific functional polymorphism in KCNMB1 shows sex-specific association with asthma severity. *Hum. Mol. Genet.* 17:2681–2690. doi:10.1093/hmg/ddn168

Stefani, E., M. Ottolia, F. Noceti, R. Olcese, M. Wallner, R. Latorre, and L. Toro. 1997. Voltage-controlled gating in a large conductance Ca2+-sensitive K+channel (hslo). *Proc. Natl. Acad. Sci. USA.* 94:5427–5431. doi:10.1073/pnas.94.10.5427

Uebele, V.N., A. Lagrutta, T. Wade, D.J. Figueroa, Y. Liu, E. McKenna, C.P. Austin, P.B. Bennett, and R. Swanson. 2000. Cloning and functional expression of two families of beta-subunits of the large conductance calcium-activated K+ channel. *J. Biol. Chem.* 275:23211–23218. doi:10.1074/jbc.M910187199

Wallner, M., P. Meera, and L. Toro. 1996. Determinant for beta-subunit regulation in high-conductance voltage-activated and Ca(2+)-sensitive K+ channels: an additional transmembrane region at the N terminus. *Proc. Natl. Acad. Sci. USA.* 93:14922–14927. doi:10.1073/pnas.93.25.14922

Wallner, M., P. Meera, and L. Toro. 1999. Molecular basis of fast inactivation in voltage and Ca2+-activated K+ channels: a transmembrane beta-subunit homolog. *Proc. Natl. Acad. Sci. USA.* 96:4137–4142. doi:10.1073/pnas.96.7.4137

Wang, B., B.S. Rothberg, and R. Brenner. 2006. Mechanism of β4 subunit modulation of BK channels. *J. Gen. Physiol.* 127:449–465. doi:10.1085/jgp.200509436

Wang, L., and F.J. Sigworth. 2009. Structure of the BK potassium channel in a lipid membrane from electron cryomicroscopy. *Nature.* 461:292–295. doi:10.1038/nature08291

Wang, Y.W., J.P. Ding, X.M. Xia, and C.J. Lingle. 2002. Consequences of the stoichiometry of Slo1 alpha and auxiliary beta subunits on functional properties of large-conductance Ca2+-activated K+ channels. *J. Neurosci.* 22:1550–1561.

Wilkinson, B., and H.F. Gilbert. 2004. Protein disulfide isomerase. *Biochim. Biophys. Acta.* 1699:35–44.

Wu, R.S., N. Chudasama, S.I. Zakharov, D. Doshi, H. Motoike, G. Liu, Y. Yao, X. Niu, S.X. Deng, D.W. Landry, et al. 2009. Location of the beta 4 transmembrane helices in the BK potassium channel. *J. Neurosci.* 29:8321–8328. doi:10.1523/JNEUROSCI.6191-08.2009

Xia, X.M., J.P. Ding, X.H. Zeng, K.L. Duan, and C.J. Lingle. 2000. Rectification and rapid activation at low Ca2+ of Ca2+-activated, voltage-dependent BK currents: consequences of rapid inactivation by a novel beta subunit. *J. Neurosci.* 20:4890–4903.

Yarov-Yarovoy, V., D. Baker, and W.A. Catterall. 2006. Voltage sensor conformations in the open and closed states in ROSETTA structural models of K(+) channels. *Proc. Natl. Acad. Sci. USA.* 103:7292–7297. doi:10.1073/pnas.0602350103